Langmuir
Article
pubs.acs.org/Langmuir

Photochromic Nanostructures Based on Diarylethenes with Perylene Diimide

Lulu Ma,[†] Quanbo Wang,[†] Guifen Lu,[§] Ruiping Chen,[‡] and Xuan Sun*,[†]

[†]*Key Laboratory of Colloid and Interface Chemistry of the Ministry of Education, School of Chemistry and Chemical Engineering, Shandong University, Jinan 250100, PR China,* [§]*School of Chemistry and Chemical Engineering, Jiangsu University, Zhenjiang 212013, PR China, and* [‡]*State Key Laboratory of Structural Chemistry, Fujian Institute of Research on the Structure of Matter, Chinese Academy of Sciences, Fuzhou 350002, PR China*

Received October 24, 2009. Revised Manuscript Received December 4, 2009

A bisthienylethene-functionalized perylene diimide (BTE-PDI) photochromic dyad was synthesized for self-assembly into 1-D nanotubes by a reprecipitation method. SEM and TEM observations showed that the nanotubes were formed from their 0-D precursors of hollow nanospheres. HR-TEM images revealed that both the nanospheres and the nanotubes have highly ordered lamellar structure, indicating the hierarchical process during assembly. The IR and XRD results revealed that DAE-PDI molecules were connected through intermolecular hydrogen bonds to form building blocks that self-assembled into nanostructures. Electronic absorption and fluorescence spectroscopic results indicated the H-aggregate nature of the self-assembled nanostructures. Competition and cooperation between the dipole−dipole interaction, intermolecular $\pi-\pi$ stacking, and hydrophilic/hydrophobic interaction are suggested to result in nanostructures. Reconstruction was found to happen during the morphology transition progress from the 0-D nanospheres to the 1-D nanotubes, which was driven by donor−acceptor dipole−dipole interactions. Green emission at 520 nm originating from the DAE subunit was observed for the aggregates of vesicles and nanotubes, which could be regulated by photoirradiation with 365 nm light, suggesting the nanoaggregates to be photochromic switches.

1. Introduction

Mediated by noncovalent interactions (e.g., hydrogen bonding interactions, $\pi-\pi$ stacking, and solvophobic and surface effects), the self-assembly of atomic/molecular building blocks into large supramolecular structures offers significant advantages in device miniaturization, which can fabricate features on the scale of a few nanometers. To date, numerous interesting materials have been constructed from a large library of molecular building blocks, among which amphiphilic molecules with controlled hydrophilic/hydrophobic interactions can hierarchically self-assemble into highly organized aggregates with a hollow interior and various morphologies, especially 0-D and 1-D micro/nano hollow spheres and tubes with unique multilevel inner structures. These multilevel structural micro/nanomaterials have spurred great attention not only because of their fantastic interior architectures but also for their unique predominance and multifunctionality that are superior to their same-sized solid counterparts.[1−7] Moreover, the fabrication of smart supramolecular materials by the introduction of stimuli-responsive groups into building blocks that are responsive to external stimuli is believed to have significant potential with respect to actuation, sensing, data storage, and computing. Whereas light represents perhaps the most attractive external stimulus, light-triggered structural changes in building blocks affect their self-assembly behavior and therefore modulate macroscopic properties, which has previously rarely been explored.[8−13] Actually, the fabrication of new functional supramolecular assemblies and materials based on photoresponsible molecular building blocks for understanding the assembly formation mechanism are still challenging tasks. Herein, we report the hierarchical supramolecular self-assembly of a photochromic molecule, a bisthienylethene (BTE) derivative, by a precipitation method. The morphology of the self-assembly formed in methanol is confirmed to be nanospheres with well-defined lamellar hollow structures. More interestingly, a morphology transition took places in the self-assembly process, which induced 0-D nanospheres to transform into 1-D nanotubes. Although the red emission of the PDI subunit is quenched by aggregation, the green emission of the DAE subunit remained strong and can be modulated by light irradiation, indicating that the material brings about potential applications in the fields of data storage and computing.

2. Experimental Section

2.1. Chemicals. Unless stated otherwise, all reagents and anhydrous solvents were purchased from Aldrich Chemicals and were used without further purification and drying except as noted. Column chromatography (CC) was used: SiO_2 (200−300

*Corresponding author. Tel: +86-531-88362326. E-mail: sunxuan@sdu.edu.cn.

(1) Percec, V.; Dulcey, A. E.; Balagurusamy, V. S. K.; Miura, Y.; Smidrkal, J.; Peterca, M.; Nummelin, S.; Edlund, U.; Hudson, S. D.; Heiney, P. A.; Duan, H.; Magonov, S. N.; Vinogradov, S. A. *Nature* **2004**, *430*, 764.
(2) Antonietti, M.; Förster, S. *Adv. Mater.* **2003**, *15*, 1323.
(3) Hill, J. P.; Jin, W. S.; Kosaka, A.; Fukushima, T.; Ichihara, H.; Shimomura, T.; Ito, K.; Hashizume, T.; Ishii, N.; Aida, T. *Science* **2004**, *304*, 1481.
(4) Hartgerink, J. D.; Beniash, E.; Stupp, S. I. *Science* **2001**, *294*, 1684.
(5) Uzun, O.; Sanyal, A.; Nakade, H.; Thibault, R. J.; Rotello, V. M. *J. Am. Chem. Soc.* **2004**, *126*, 14773.
(6) Arnt, L.; Tew, G. N. *J. Am. Chem. Soc.* **2002**, *124*, 7664.
(7) Percec, V.; Ahn, C. H.; Ungar, G.; Yeardley, D. J .P.; Moüller, M.; Sheiko, S. S. *Nature* **1998**, *391*, 161.
(8) Murata, K.; Aoki, M.; Nishi, T.; Ikeda, A.; Shinkai, S. *J. Chem. Soc., Chem. Commun.* **1991**, 1715.
(9) Murata, K.; Aoki, M.; Suzuki, T.; Harada, T.; Kawabata, H.; Komori, T.; Ohseto, F.; Ueda, K.; Shinkai, S. *J. Am. Chem. Soc.* **1994**, *116*, 6664.
(10) Loos, M. D.; Esch, J. V.; Kellogg, R. M.; Feringa, B. L. *Angew. Chem., Int. Ed.* **2001**, *40*, 613.
(11) Laan, S. V. D.; Feringa, B. L.; Kellogg, R. M.; Esch, J. V. *Langmuir* **2002**, *18*, 7136.
(12) Jong, J. J. D. D.; Lucas, L. N.; Kellogg, R. M.; Esch, J. H. V.; Feringa, B. L. *Science* **2004**, *304*, 278.
(13) Hirose, T.; Matsuda, K.; Irie, M. *J. Org. Chem.* **2006**, *71*, 7499.

mesh). 2,3-Bis(2,3,5-trimethyl-3-thienyl) maleic anhydride was prepared following a literature procedure.[14] *N*,*N*′-diamido-1,6,7,12-tetra(4-tert-butylphenoxy)perylene-3,4/9,10-tetracarboxylic acid bisimide was prepared according to a procedure similar to that in the literature.[15]

2.2. Synthesis of BTE-PDI Dyad 1. Synthesis of the target BTE-PDI **1** was accomplished in one step by the condensation of photochromic 2,3-bis(2,3,5-trimethyl-3-thienyl) maleic anhydride with a stoichiometric amount of the corresponding *N*,*N*′-diamido-1,6,7,12-tetra(4-tert-butylphenoxy)perylene-3,4/9,10-tetracarboxylic acid bisimide in refluxing toluene in the presence of imidazole as a catalyst. Details of the synthesis will be described and published elsewhere.

2.3. Evaporation Method. The sample was dissolved in $CHCl_3$ to a concentration of 10^{-3} mol·L^{-1}. The solution (100 μL) was injected into 3 mL of anhydrous methanol (described as $CHCl_3/CH_3OH$ (v/v = 1/30) in the text). After the solution was allowed to equilibrate over 3 h, 4 to 5, and 6 h at 38 °C, one drop of solution was cast onto the carbon copper grids in order to observe the aggregate behavior in the solid state. CH_3OH was also converted to acetone or THF when the assemblies were manufactured. The nanospheres collected from the suspension were held at 50 °C for 10 min to evaporate the CH_3OH, and the nanostructure collapsed.

2.4. Characterization. ^{1}H NMR spectra were recorded on a Bruker DPX 300 spectrometer (300 MHz) in $CDCl_3$ using the residual solvent resonance of $CHCl_3$ at 7.26 ppm relative to $SiMe_4$ as an internal reference. Matrix-assisted laser desorption/ionization time-of-flight (MALDI-TOF) mass spectra were detected on a Bruker BIFLEX III ultrahigh-resolution Fourier transform ion cyclotron resonance (FT-ICR) mass spectrometer with α-cyano-4-hydroxycinnamic acid as the matrix. Elemental analyses were performed by the Institute of Chemistry at the Chinese Academy of Sciences. Fourier transform infrared spectra (FT-IR) were recorded for KBr pellets with 2 cm^{-1} resolution using a VERTEX-70 (Bruker) spectrometer. Absorption spectra were measured on a Hitachi U-4100 spectrophotometer. Steady-state fluorescence measurements of a $CHCl_3$ and $CHCl_3/CH_3OH$ combined solution of the BTE-PDI compound were performed on a fluorescence spectrophotometer (Perkin-Elmer LS-50) with excitation at a wavelength of 488 nm, and the emission spectrum between 500−700 nm was recorded. A fluorescence microscopy image of the aggregates was obtained with a mercury lamp and a 40× objective and captured with a DP70 CCD camera (Japan) on an Olympus FV 500 instrument (Japan). Excitation was performed with the Ar 488 nm laser, and the emission was monitored from 600 to 800 nm. Standard lamps used to visualize TLC plates (Spectroline E-series, 470 μW/cm^2) were used to carry out the ring-closing reaction of **1o** to **1c**. Transmission electron microscopy images were recorded on a JEOL-100CX II electron microscope operated at 100 kV. A high-resolution transmission electron microscopy (HR-TEM) measurement was performed with a JEOL-2010 working at 200 kV. Scanning electron microscopy images were obtained on a JEOL JSM-6700F. The powder X-ray diffraction (XRD) patterns were recorded using a Rigaku D/Max 2200-PC diffractometer with Cu Kα radiation (λ = 0.15418 nm) and a graphite monochromator at ambient temperature. For TEM and HR-TEM imaging, a drop of sample solution was cast onto a copper grid sprayed with carbon. For SEM imaging, Au (1 to 2 nm) was sputtered onto these grids to prevent charging effects and improve image clarity. All calculations were carried out with the density functional theory (DFT) method at the B3LYP/LANL2DZ and B3LYP/(6-31+G*, LANL2DZ) levels. All of the calculations were performed using Gaussian 03 program 27 in the IBM P690 system at the Shandong Province High Performance Computing Centre.

(14) Irie, M.; Mohri, M. *J. Org. Chem.* **1988**, *53*, 803.
(15) Würthner, F.; Thalacker, C.; Sautter, A. *Adv. Mater.* **1999**, *11*, 754.

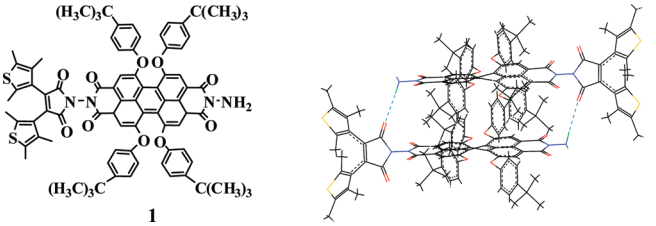

1

Figure 1. Schematic illustration of the chemical structure of BTE-PDI **1** and the possible intermolecular translation-related hydrogen bonding.

3. Results and Discussion

3.1. Molecule Design. As shown in Figure 1, photochromic BTE is covalently linked to the bay-substituted perylene tetracarboxylic acid bisimide (PDI) on the amino N atom to form the functional structure of light-regulated fluorescence-switching **1**.[16] Drastic fluorescence quenching of BTE-PDI dyad **1** compared with reference compound *N*,*N*′-dibutyl-1,6,7,12-tetra(4-tert-butylphenoxy)pery-lene-3,4/9,10-tetracarboxylic diimide indicates rapid electron transfer from the $-NH_2$ group to the tetraphenoxy-substituted PDI within this intramolecular charge-transfer (ICT) compound, $NH_2^{\bullet+}-PDI^{\bullet-}-$BTEo (open state of BTE).[17] Furthermore, polar amino moiety $-NH_2$ remained unsubstituted to exhibit a hydrophilic effect relative to the solvophilic skeleton of BTE-PDI **1**, hence the amphiphilic structure can facilitate the self-assemble process. Besides, the PDI segment has a strong tendency to aggregate through $\pi-\pi$ overlap, and the intermolecular hydrogen bonding has a synergistic effect on the formation of extremely stable aggregations. The unique structural feature of BTE-PDI **1** makes it an ideal candidate for self-assembly using the synergistic effects of $\pi-\pi$ stacking, microsegregation, intermolecular hydrogen bonding, and dipole−dipole interaction.

3.2. Self-Assembly of Molecule 1. The aggregation behavior of **1** was subsequently studied by injecting a chloroform ($CHCl_3$) solution of **1** into methanol (CH_3OH) to give a final $CHCl_3/CH_3OH$ ratio of 1/30 (v/v). It is important to note that the growth time played a key role in controlling the self-assembly process starting from the hollow nanospheres to the tadpolelike vesicles and nanotubes. Figure 2 shows typical scanning electron microscopy (SEM) and the corresponding transmission electron microscopy (TEM) images of **1** with different morphologies. After the solution was allowed to equilibrate for 3 h at 38 °C, one drop of the solution was evaporated on the carbon-coated grid to observe the aggregate behavior in the solid state. Irregular spherical particles with small defects on the surface are observed in the SEM images (Figure 2a). The diameter of the spheres ranges from 800 to 2800 nm. TEM observation (Figure 2b) confirms that all of the spherical structures are hollow in nature with a wall thickness of roughly 20−350 nm. Not occasionally, as revealed in SEM and TEM images (Figure 2a,b), vesicles are not separately dispersed but cohered one-by-one in a linear way, forming "pearl necklace" morphology. The adjacent vesicles fuse with one another and the membranes between them are eroded, suggesting the growing tendency of the tubes.

To investigate this tendency, the sample in the combined $CHCl_3/CH_3OH$ solvents system is aged for 1 h more and the intermediate states of the morphology transition are obtained. Many discrete 0-D and 1-D nanostructures are observed (Figure 3). The typical structure of the intermediates is tadpolelike

(16) Fukaminato, T.; Irie, M. *Adv. Mater.* **2006**, *18*, 3225.
(17) Würthner, F.; Thalacker, C.; Diele, S.; Tschierske, C. *Chem.—Eur. J.* **2001**, *7*, 2245.

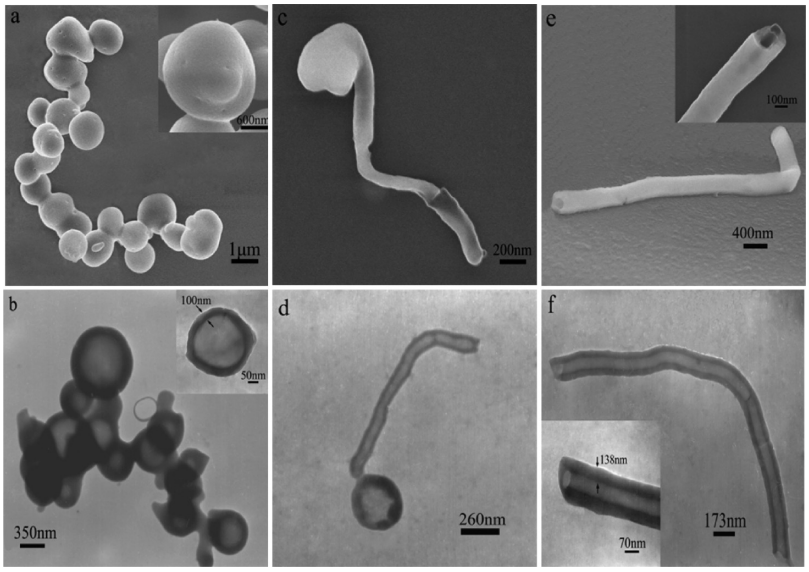

Figure 2. Typical morphologies of the nanostructures formed by injecting the $CHCl_3$ solution of **1** into CH_3OH. (a) SEM of the nanospheres formed within 3 h. (b) TEM of the nanospheres. (c) SEM of the nanotadpoles formed around 4 h. (d) TEM of the nanotadpoles. (e) SEM of the nanotubes formed after 5 h. (f) TEM of the nanotubes.

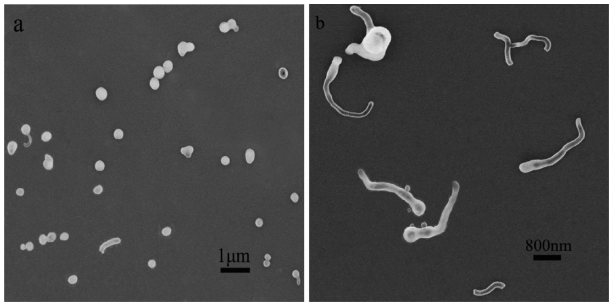

Figure 3. SEM photography of the nanostructures formed by injecting the $CHCl_3$ solution of **1** into CH_3OH and equilibrating for 5 h. (a) SEM image with many 0-D nanostructures and (b) SEM image with many 1-D nanostructures.

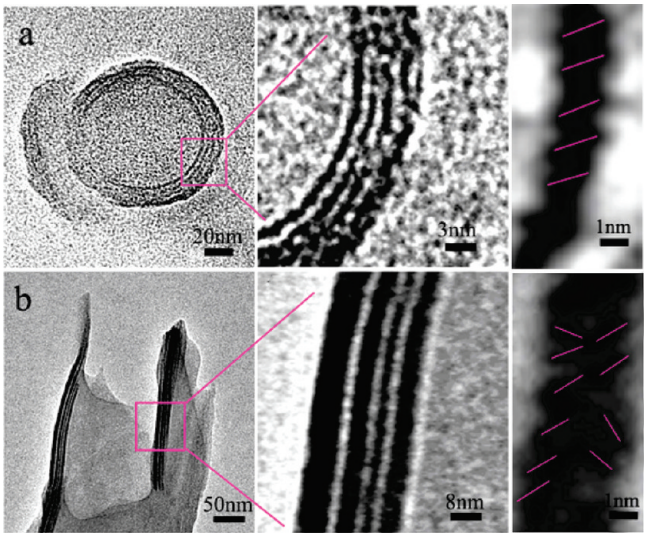

Figure 4. HR-TEM images of typical nanospheres and nanotubes formed in $CHCl_3$ and CH_3OH (volume ratio = 1/30). (a) HR-TEM image of the nanospheres and the magnification of the interlamellar structure of the shell. (b) HR-TEM image of the nanotubes as well as the amplified structure of the tubular shell.

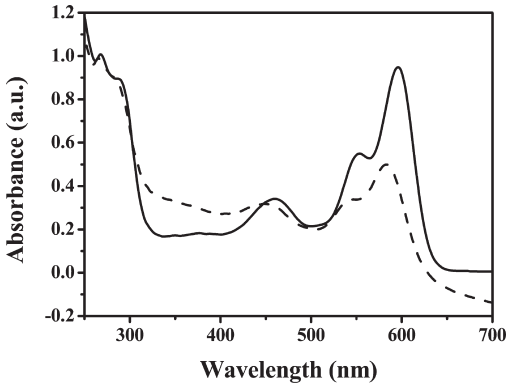

Figure 5. Electronic absorption spectra of **1** in $CHCl_3$ (5×10^{-5} mol·L^{-1}, −) and its self-assembled nanoscale aggregates formed in $CHCl_3/CH_3OH$ (v/v = 1/30, ---).

morphology with a hollow spherical head and a tubular tail, formed by the corrosion of the membranes between the pearls (Figure 2c,d), clearly indicating the 1-D growing process. Nanotubes with a length of more than 8 μm are obtained by the long-time stabilization (left undisturbed for more than 5 h at 38 °C) of the precipitate (Figure 2e,f), which again confirms the 1-D growth tendency of the vesicles. The surface of the tubes is relatively smooth and the inner and outer diameters are uniform with a wall thickness of about 135−150 nm. The progressive growth of the assembly from vesicles to nanotubes was a natural process that depended only on time and was similar to some natural biological growth phenomena. These results provide a very interesting artificial molecular system in which to mimick the features of growth in natural systems.

Insight into the aggregation behavior of **1**, the well-ordered lamellar structure, can clearly be identified from the HR-TEM (high-resolution transmission electron microscopy) micrograph of a single hollow nanosphere (Figure 4a). The membrane wall contains several lamellas in interspaces of the solvents, as illustrated in the enlarged image. The average thickness of each ridge (darkness in Figures) is roughly 1.7 nm. Interestingly, the molecular arrangement can almost be identified from the magnified

image (Figure 4a). According to the thickness of one ridge and the dimensions of an optimized molecule, molecules may stack oppositely by intermolecular hydrogen bonding and $\pi-\pi$ interactions estimated by the 3-D molecular structural modeling (Figure 1). One lamella containing two ridges and one interspace (1.6 nm) (whiteness in Figures) is measured to be about 5.0 nm, corresponding to the *d* spacing of the X-ray diffraction results (XRD, Figure 6). This lamella structure clearly indicates that molecules of **1** are arranged in an orderly manner into a monolayer by noncovalent interactions. When such a monolayer is formed, extra CH_3OH molecules in the organic solvent could be attracted through hydrogen bonding to **1** or by the permanent dipole in the layer. Therefore, a repetition of the above process generates stacked multilayers, as illustrated in Figure 4a.

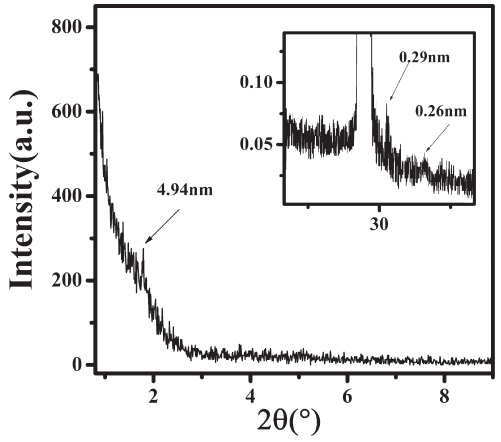

Figure 6. XRD profiles of the hollow nanospheres of **1**.

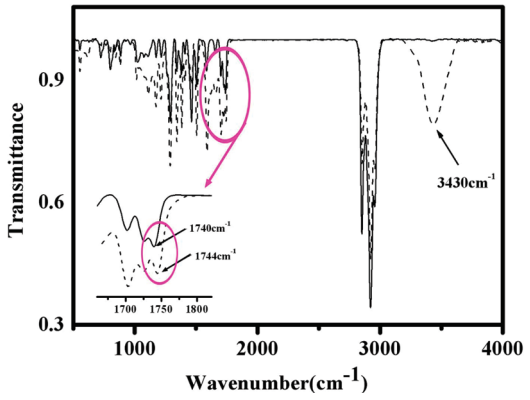

Figure 7. IR spectra of **1** (—) and aggregates (---) in the 400−4000 cm^{-1} region with 2 cm^{-1} resolution.

The HR-TEM image of the nanotubes shows the hollow interiors of the 1-D structures with a well-defined laminate structure of the wall (Figure 4b). The width of the striped domains is not uniform, with the thickness of the ridges ranging from 2.0 to 8.0 nm, which can be attributed to the amalgamation of several ridges and the loss of interspaces. The homology of the structure between the nanovesicles and the nanotubes indicates the uniform nature of the two nanostructures, which again reveals the morphology transition process from the 0-D nanospheres to the 1-D nanotubes.

UV/vis absorption spectroscopy and X-ray diffraction are used to clarify the packing of the molecules in the self-assembled aggregates. Figure 5 displays the electronic absorption spectrum of **1** in $CHCl_3$ as well as that in combined solvents of $CHCl_3$ and CH_3OH. The aggregation of **1** leads to pronounced changes in the optical properties with a blue shift (13 nm) relative to that of the monomeric PDI unit, suggesting that, in spite of the large steric hindrance induced by the bulky substitutes at the bay positions, the molecules pack face-to-face with considerable overlap between the adjacent PDI aromatic rings, which is distinct for the generally observed *J*-type aggregates of the tetraphenoxy-substituted PDIs.[5] Such spectroscopic changes arising from the formation of the aggregates are attributed to the efficient $\pi-\pi$ interaction that proceeds from the ordered molecular packing as visualized in the HR-TEM results (Figure 4). By prolonging the aging time of the sample in $CHCl_3/CH_3OH$ solution to longer than 6 h, no changes in the absorption spectra are observed, which may indicate that molecules arrange in the same manner in the vesicles and nanotubes.

The XRD pattern of the self-assembled vesicles (Figure 6) shows one diffraction peak at $2\theta = 1.79°$, which can be ascribed to the refraction from the lamellar structure of the hollow shell. The *d* spacing is therefore 4.94 nm, representing the distance of two layers containing one interlayer of the lamellar structure, which is in good agreement with the HR-TEM observation (Figure 4a). The inset in Figure 6 demonstrates the diffraction

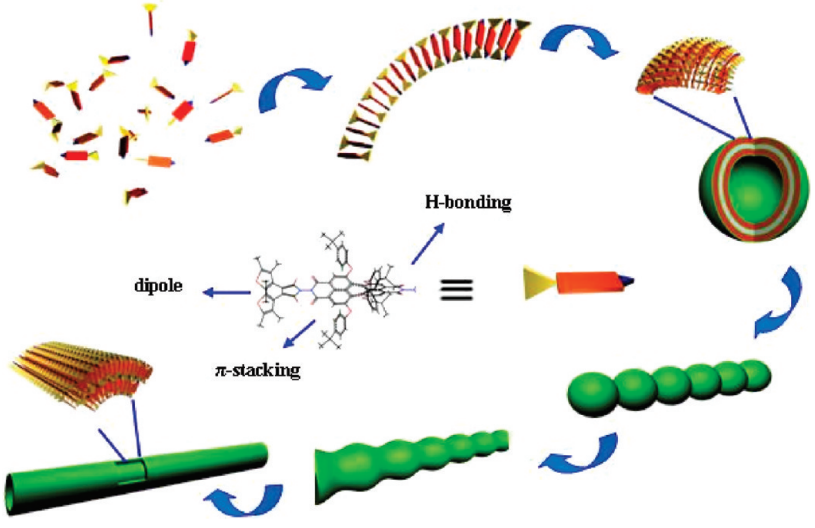

Figure 8. Schematic illustration of nanostructure formation from **1** and the morphology-transition process.

in the wide-angle range, where weak peaks at $2\theta = 30.76$ and 34.72° are observed and are attributed to the $\pi-\pi$ stacking and average hydrogen bonding distance between neighboring molecules, respectively.[18] These results, together with the HR-TEM observation and the electronic absorption spectrum, indicate that the molecules form ordered H aggregates in the membrane of the hollow nanostructures by the synergic $\pi-\pi$ and hydrogen bonding interactions.

The FT-IR spectra of **1** as well as that of the nanoaggregates are compared in Figure 7. The relatively strong, broad band appeared at 3435 cm^{-1} in the spectrum of the aggregates, which is absent from that of **1**, apparently originated from the hydrogen bonding stretching vibration.[18−20] In addition, the characteristic C═O stretching vibration of the BTE subunit in the aggregates shifts upfield compared with that in **1**, which is ascribed to the weakening of the p$-\pi$ conjugation between the lone-pair electron on oxygen and the thiophene caused by hydrogen bonding. Therefore, the formation of hydrogen bonds between the C═O parts of the BTE units and the $-NH_2$ groups of the PDIs is proposed as illustrated in Figure 1. These changes clearly demonstrate the significant effect of the hydrogen bonding interaction on the formation of molecular aggregates.

3.3. Possible Mechanism for the Formation of the Nanostructures of 1. On the basis of the above-described experimental results, a possible assembly mechanism is thus proposed as shown in Figure 8,[21] including the following steps: (1) neighboring BTE-PDI molecules are connected through charge−charge interaction, hydrogen bonding, and $\pi-\pi$ interactions to form clusters acting as building blocks; (2) various building blocks grow into nano- or microscale assemblies with hollow vesicle morphology by microphase segregation, and (3) the 0-D hollow nanospheres transform into 1-D nanotubes by the dipole−dipole driving force and the evaporation of methanol.

As disclosed, for such a strongly polar compound as **1**, charge−charge interactions have a dominating influence on the packing geometry.[17] Repulsion and attraction between the adjacent $\pi-\pi$ stacked molecules and the steric demand of the substituents in the bay positions lead to a longitudinal offset. Moreover, in the case of **1**, intermolecular hydrogen bonding is required in forming the large overlapped H aggregates as demonstrated in the HR-TEM observation (Figure 4a) and simulated in Figure 1. Meanwhile, the lamella morphology of the nanostructures membrane indicates that microphase separation plays an important role in the molecular self-assembly process, which is always found in micellar or tube formation of amphiphilic molecules.[2,22] The relatively wide interlayer between two adjacent layers as well as the irregular morphology and rough surface of the nanospheres may indicate that the building blocks stack in a relatively loose manner. CH_3OH may play a specific role in the formation of the lamella structure because no tangible morphology can be obtained by changing the CH_3OH into acetone or tetrahydrofuran when manufacturing the assemblies. Upon heating, especially when the temperature arrived at 50 °C, the nanospheres collapsed with the evaporation of CH_3OH, which may verify the important effect of CH_3OH on the molecular self-assembly.[23]

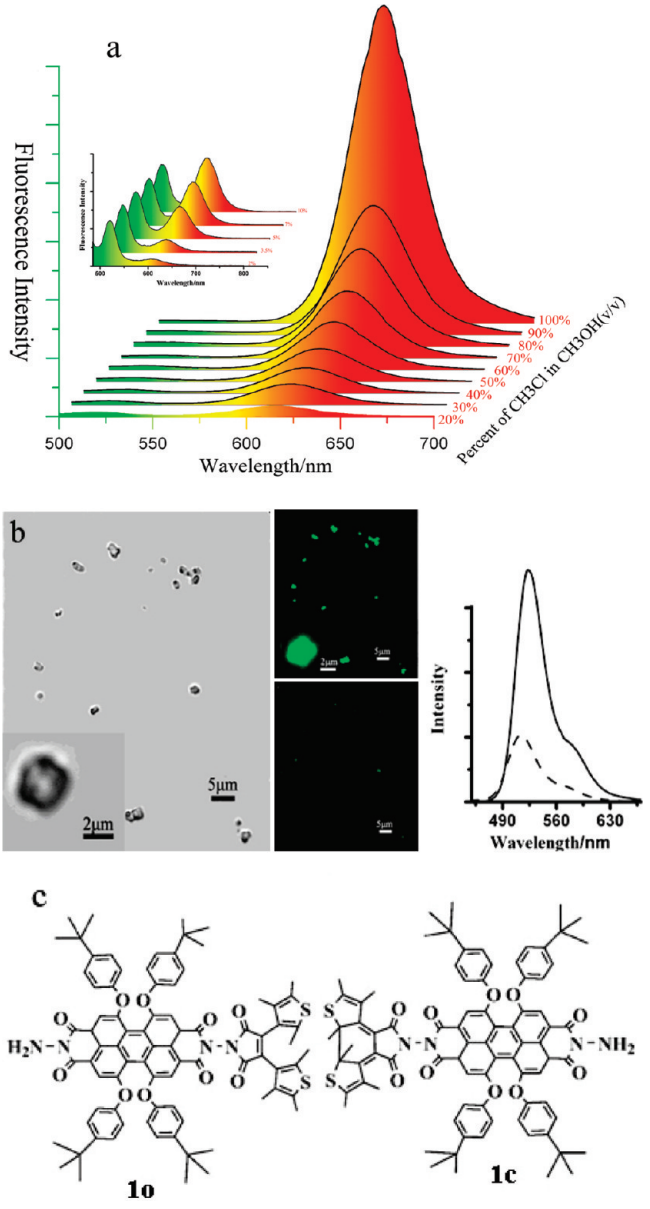

Figure 9. (a) Fluorescence spectra of **1** in $CHCl_3$ and a $CHCl_3$/CH_3OH combined solvent system, with $\lambda = 488$ nm and [BTE-PDI **1**] $= 3.0 \times 10^{-6}$ mol·L^{-3}. The inset shows the fluorescence spectra of **1** in $CHCl_3$ in CH_3OH (v/v) from 2 to 10%. (b) Confocal fluorescence images and fluorescence spectral changes of aggregates of BTE-PDI **1** before (relative strong emission, −) and after (very weak emission, ---) photoirradiation with 365 nm light for 10 min. (c) Schematic representation of the structures of the open form **1o** (PDI-BTEo) and the closed-form **1c** (PDI-BTEc).

Considering the molecular structure of **1**, the dipole−dipole interaction is proposed to be the dominating driving force for the morphology transition from 0-D to 1-D, similar to the 1-D growing progress of an ICT compound.[24−28] For **1**, the main transition dipole moment is along the long molecular axis

(18) Lu, G. F.; Chen, Yanli; Zhang, Y. X.; Bao, M.; Bian, Y. Z.; Li, X. Y.; Jiang, J. Z. *J. Am. Chem. Soc.* **2008**, *130*, 11623.
(19) Kimura, M.; Muto, T.; Takimoto, H.; Wada, K.; Ohta, K.; Hanabusa, K.; Shirai, H.; Kobayashi, N. *Langmuir* **2000**, *16*, 2078.
(20) Kimura, M.; Kuroda, T.; Ohta, K.; Hanabusa, K.; Shirai, H.; Kobayashi, N. *Langmuir* **2003**, *19*, 4825.
(21) Xu, J. L.; Liu, X. F.; Lv, J.; Zhu, M.; Huang, C. S.; Zhou, W. D.; Yin, X. D.; Liu, H. B.; Li, Y. L.; Ye, J. P. *Langmuir* **2008**, *24*, 4231.
(22) Yan, D. Y.; Zhou, Y. F.; Hou, J. *Science* **2004**, *303*, 65.
(23) Huang, C. S.; Wen, L. P.; Liu, H. B.; Li, Y. L.; Liu, X. F.; Yuan, M. J.; Zhai, J.; Jiang, L.; Zhu, D. B. *Adv. Mater.* **2009**, *21*, 1.
(24) Xu, J. L.; Wen, L. P.; Zhou, W. D.; Lv, J.; Guo, Y. B.; Zhu, M.; Liu, H. B.; Li, Y. L.; Jiang, L. *J. Phys. Chem. C* **2009**, *113*, 5924.
(25) Zhang, X. J.; Zhang, X. H.; Shi, W. S.; Meng, X. M.; Lee, C. S.; Lee, S. T. *Angew. Chem., Int. Ed. Engl.* **2007**, *46*, 1525.
(26) Zhang, X. J.; Zhang, X. H.; Zou, K.; Lee, C. S.; Lee, S. T. *J. Am. Chem. Soc.* **2007**, *129*, 3527.
(27) Zhang, C. Y.; Zhang, X. J.; Zhang, X. H.; Fan, X.; Jie, J. S.; Chang, J. C.; Lee, C. S.; Zhang, W. J.; Lee, S. T. *Adv. Mater.* **2008**, *20*, 1716.
(28) Yamamoto, Y.; Fukushima, T.; Suna, Y.; Ishii, N.; Saeki, A.; Seki, S.; Tagawa, S.; Taniguchi, M.; Kawai, T.; Aida, T. *Science* **2006**, *314*, 1761.

(Figure 8,[21]), according to the calculation results and consistent with the results interpreted by Würthner et al.,[17] which will direct the morphology transition process. Besides, the dipole−dipole interaction between the stacked thiophene rings should facilitate the transition simultaneously.[29] Therefore, concomitant with the evacuation of the solvent interspace, dipole−dipole interactions act as the major forces driving layers in 0-D structure to fuse together and finally direct the formation of 1-D nanotubes. The fusion of vesicles released the curvature energy, leading to a thermodynamically more stable tubular structure.

3.4. Photochromic Properties of the Assemblies. A fluorescence study is carried out to investigate the assembly behavior as well as the switching performance of the aggregates. As shown in Figure 9a, the emission spectra of molecularly dissolved **1** display a mirror-image relationship to the absorption spectrum with a large Stokes' shift (25 nm) in $CHCl_3$. Upon addition of CH_3OH to the $CHCl_3$ solution, a gradual decrease in fluorescence intensity with a maximum at 619 nm was observed, indicating the presence of a fluorescence quenching effect induced by the strong intermolecular $\pi-\pi$ stacking as a result of aggregate formation.[30−35] When the ratio of the $CHCl_3$ to CH_3OH reaches 3%, of which the well-defined nanostructures (nanospheres and nanotubes) formed, the emission at 619 nm originating from the PDI core was quenched almost completely whereas the emission at 520 nm is observed (inset in Figure 9a). According to the relative BTE compound investigated previously,[36] the emission with a maximum at 520 nm is ascribed to the fluorescence of the open form of 2,3-bis(2,3,5-trimethyl-3-thienyl)maleic anhydride.

The response of the assemblies to light stimulation is studied by confocal fluorescence microscopy. As displayed in Figure 9b, particles with dimension of about 1 to 2 μm with bright-green emission are observed. This green emission is therefore ascribed to the fluorescence of the BTE components within the aggregates, corresponding to the fluorescence spectra of the assembly mentioned above. Upon irradiation of the aggregates with 365 nm light for 10 min, the green emission is dramatically quenched, suggesting that an efficient molecular photocyclization-induced (as shown in Figure 9c) photochromic transformation arises in the assembled structures and revealing the superiority of the assemblies over the colloidal solutions and amorphous films.[37] The "on" and "off" emission modulated by light stimuli indicates that the material is a good switch bearing great potential in the fields of information storage and computing. Details of the photochromic reaction-induced conformational changes of **1** and the subsequent light-controlled assembly alteration are being carried out in our laboratory and will be published elsewhere.

4. Conclusions

A diarylethene-functionalized perylene diimide (BTE-PDI) photochromic dyad has been designed and self-assembled into aggregates by a reprecipitation method. Vivid SEM and TEM images were recorded and confirmed that the molecules are able to self-assemble into 0-D vesicles and thereafter continually grow into 1-D tubes. Both the vesicles and the tubes have highly ordered lamellar structure, indicating the hierarchical process during assembly formation. The fluorescence of the vesicles can be regulated by photoirradiation with UV light, suggesting the aggregates to be good photochromic switches. These findings provide a simple method for the introduction of stimuli-responsive groups into building blocks to fabricate dynamic and smart devices on the scale of nanometers, and the progressive growth demonstrates a promising pathway for constructing an artificial system that mimicks the features of growth in nature.

Acknowledgment. We are grateful for financial support by the Nature Science Foundation of Shandong Province (Y2006B14) and a grant from the Ph.D. Programs Foundation of the Ministry of Education of China.

(29) Saita, K.; Kobatake, S.; Fukaminato, T.; Nanbu, S.; Irie, M.; Sekiya, H. *Chem. Phys. Lett.* **2008**, *454*, 42.
(30) Liu, S. G.; Sui, G. D.; Cormier, R. A.; Leblanc, R. M.; Gregg, B. A. *J. Phys. Chem. B* **2002**, *106*, 1307.
(31) Yan, P.; Chowdhury, A.; Holman, M. W.; Adams, D. M. *J. Phys. Chem. B* **2005**, *109*, 724.
(32) Zhang, X.; Chen, Z. J.; Würthner, F. *J. Am. Chem. Soc.* **2007**, *129*, 4886.
(33) Schneider, M.; Hangen, J.; Haarer, D.; Müllen, K. *Adv. Mater.* **2000**, *12*, 351.
(34) Tang, T. J.; Qu, J. Q.; Müllen, K.; Webber, S. E. *Langmuir* **2006**, *22*, 26.
(35) Gregg, B. A. *J. Phys. Chem. B* **2003**, *107*, 4688.
(36) Me, M.; Sayo, K. *J. Phys. Chem.* **1992**, *96*, 7671.
(37) Kasatani, K.; Kambe, S.; Irie, M. *J. Photochem. Photobiol., A* **1999**, *122*, 11.